Assessment of flow forces on large wood in rivers

F. Douglas Shields Jr.[1] and Carlos V. Alonso[1,2]

Received 21 October 2011; revised 2 March 2012; accepted 7 March 2012; published 17 April 2012.

[1] Large wood (LW) exerts an important influence on the geomorphology and ecology of streams and rivers. The magnitudes of flow forces on LW are needed to support stream management activities and are typically computed using time mean lift and drag coefficients determined in laboratory flumes using small, smooth cylinders. Herein we report measurements of forces on LW of varying complexity (simple cylinder, branching, and complex root wad) and surface (bark) roughness made in an outdoor grassed channel under steady and unsteady flows. LW orientation relative to the primary flow direction and LW relative submergence were varied. Drag and lift coefficients for cylindrical (unbranched) LW followed patterns reported by others for metal cylinders in wind tunnels. Drag coefficients for cylindrical (unbranched) LW, corrected for blockage effects, ranged from −0.05 to 1.29, and lift coefficients ranged from −0.88 to 0.52, varying systematically with LW position relative to the channel bed and incident flow direction. Measured drag coefficients for the noncylindrical LW, corrected for blockage effects, ranged from 0.22 to 6.27, while lift coefficients varied from −3.65 to 30.84. Systematic relationships between the relative submergence and orientation of branching LW and the drag and lift coefficients were not observed, but coefficients were greatest for LW with few branches and converged on smaller values typical of blunt bodies as LW complexity increased. For both simple and complex LW, maximum lift and drag forces during the rising limb of unsteady flows were about 2–3 times greater than steady flow temporal mean values.

Citation: Shields, F. D., Jr., and C. V. Alonso (2012), Assessment of flow forces on large wood in rivers, *Water Resour. Res.*, *48*, W04516, doi:10.1029/2011WR011547.

1. Introduction

[2] Large wood (LW, logs with diameters >10 cm and >2 m long) is widely recognized as a major component of fluvial ecosystems [*Gregory et al.*, 2003], providing essential substrate for macroinvertebrates [*Benke et al.*, 1985] and cover, velocity shelter, and scour pools for higher-level organisms such as fish [*Lester and Boulton*, 2008]. Wood obstructions influence channel hydraulics [*Gippel*, 1995; *Daniels and Rhoads*, 2003; *Mutz*, 2003; *Shields et al.*, 2003] and retention of particulate carbon [*Shields et al.* 2008a]. Retention zones provided by LW obstructions are essential habitat components in sand bed streams because of the small magnitude of hyporheic exchange [*Stofleth et al.*, 2008]. Wood is associated with morphologic processes across a range of scales: local scour [*Beebe*, 2000; *Wallerstein*, 2003, *Borg et al.*, 2007], sediment storage [*Thompson*, 1995; *Cordova et al.*, 2006] and bed material sorting [*Assani and Petit*, 1995] at the scale of a few meters up to step pool formation at reach scales in steep, forest streams to controls on channel avulsion, planform and floodplain formation in large rivers [*Triska*, 1984; *Gurnell et al.*, 2002; *Sear et al.*, 2010]. LW input to incising channel systems may provide negative feedback and prompt natural recovery [*Shields et al.*, 2000; *Erskine et al.*, 2010] and a possible template for incised channel rehabilitation projects [*Shields et al.*, 2008b; *Brooks et al.*, 2006]. Removal of wood from North American rivers, both as a direct management action and indirectly through beaver trapping, was one of the earliest and perhaps most significant impacts of European settlement [*Naiman et al.*, 1994].

[3] Riverine large wood has received much attention in recent years, with detailed analyses of LW storage and transport at reach [*Gippel et al.*, 1996], watershed [*Merten et al.*, 2010; *Downs and Simon*, 2001; *Seo et al.*, 2010], and regional [*Fremier et al.*, 2010; *Cordova et al.*, 2006] scales. Although large-scale analyses have relied on empirical associations (such as an inverse relationship between LW retention and the LW length:channel width ratio), process-based analyses require estimation of fluid forces on wood, namely buoyancy, lift and drag [*Braudrick and Grant*, 2000; *Wallerstein et al.*, 2001; *Buxton*, 2010]. Fish habitat rehabilitation using introduced large wood is widely practiced [*Roni et al.*, 2008; *Nagayama and Nakamura*, 2010], and force-balance analyses are required for designing LW habitat structures or managing naturally input LW [*Shields et al.*, 2004, 2006; *D'Aoust and Millar*, 2000; *Shields and Wood*, 2007]. Drag analyses have been used to assess effects of LW on flow resistance [*Shields and Gippel*, 1995] and to partition flow resistance among LW and other fluvial components [*Wilcox et al.* 2006].

[4] Drag and lift coefficients needed for force-balance analyses are based on judgment or results of small-scale flume experiments using cylinders or simple LW models

[1]National Sedimentation Laboratory, ARS, USDA, Oxford, Mississippi, USA.
[2]Retired.

This paper is not subject to U.S. copyright.
Published in 2012 by the American Geophysical Union

[*Braudrick and Grant*, 2001; *Cherry and Beschta*, 1989] or from laboratory studies of small cylinders in flows of air or water next to smooth boundaries. Existing data are somewhat confusing, with values for drag coefficient ranging from 0.3 to 9.0 recommended or reported [*D'Aoust and Millar*, 2000; *Manners et al.*, 2007; *Shields and Wood*, 2007]. There is a need to compare the resulting data with measurements in deeper water flows over rough boundaries and to examine drag and lift coefficients for LW with complex, branching geometry. Most previous studies of LW lift and drag report time mean coefficients. While this approach is sensible when relating lift and drag to LW geometry, orientation, or flow conditions, actual entrainment of LW is a function of instantaneous forces and designers must select safety factors that reflect likely maxima. Thus variability of lift and drag under fully turbulent flow conditions is also of interest.

[5] Below we present a description of a near-prototype-scale experimental setup for measuring flow forces on LW specimens. Drag and lift coefficients based on a series of measurements on smooth and rough cylindrical LW are presented and compared to values obtained by others using smooth cylinders in wind tunnels or flumes with smooth boundaries. Next, the temporal distributions of flow forces observed under unsteady flow loadings and for noncylindrical LW specimens using the same experimental setup are presented. Potential applications are discussed.

2. Methods and Materials

2.1. Experimental Setup

[6] The experiments were conducted in an outdoor grass-lined channel operated by the USDA Agricultural Research Service in Stillwater, Oklahoma [*Temple*, 1999]. This is a 137 m long trapezoidal channel lined with Kentucky-31 fescue, having a 1 m bankfull depth, a 1.8 m wide bed, 1V:2.3H side slopes and an average bed slope of 0.33 percent in the testing reach. The grass was mowed down to a height of roughly 0.10 m prior to the runs, discharge was monitored with an upstream Parshall flume, and the downstream depth controlled with an adjustable weir. Manning n values were approximately 0.03 for all tests [*Temple*, 1999]. Water depth was monitored along the channel with pressure transducers, and velocities were measured intermittently during steady flow with an Ott current meter and wading rod manually deployed from an instrument bridge and continuously during all flows using acoustic Doppler devices placed on the channel bed (depth-averaged velocity at channel centerline). LW specimens were mounted on a test stand placed at an instrument bridge located 46 m downstream from the channel entrance (Figure 1). Flow forces were measured during prolonged steady flows and also during rising and falling limbs of selected unsteady flow events. The run parameters for all steady flow tests are listed in Table 1 where Q is the rate of discharge, h is the flow depth above the channel bed, A is the cross-sectional flow area, U_0 is the average upstream flow velocity (Q/A).

[7] An exact determination of LW drag and lift coefficients presents a challenging problem because the locations of the separation points of wakes oscillate, causing alternating vortex shedding and force fluctuation independent of the ambient flow. Furthermore, the three-dimensionality of this phenomenon is compounded by the complexity of the incident flow [*Knight et al.*, 1994]. The most common approach for dealing with the force fluctuations is to report them in terms of time mean coefficients, while the three-dimensionality feature is similarly handled by quantifying the time mean coefficients as spatial mean values over the entire LW formation expressed in terms of a characteristic velocity [*Garcia et al.*, 2004]. Since our LW test specimens occupied only the central part (flat bed) region of the trapezoidal channel, velocity distributions published by *Knight et al.* [1994] (confirmed by comparison to distributions measured manually in our test channel) were used to convert the bulk flow velocity (Q/A) to the depth-averaged velocity for the central part of the channel, which was equivalent to the depth-averaged velocity averaged over the length of the log. The time mean of this velocity, $\overline{U}_d$,

Figure 1. (a) Upstream facing view of grass-lined outdoor channel showing the instrument bridge, test stand, and mounted log. (b) Hackberry log mounted on test stand and view of log elevation and yaw controls.

Table 1. Flow Parameters Used in the Steady Flow Large-Wood (LW) Tests

Test Date	Discharge, Q^a ($m^3 s^{-1}$)	Flow Depth, h^b (m)	Cross-Sectional Area, A^a (m^2)	Q/A, $U_0{}^a$ ($m s^{-1}$)	Froude Number[b]	Depth-Averaged Velocity, $\overline{U}_d{}^b$ ($m s^{-1}$)	LW Specimens
June 2004	3.47	0.83	3.10	1.12	0.43	1.23	Cylindrical—PVC, Oak, Hackberry
October 2005	2.07	0.83	3.08	0.67	0.26	0.74	Logs with branches and root wad
October 2005	3.43	0.85	3.16	1.09	0.42	1.20	Logs with branches and root wad

[a]Based on entire cross section of flow.
[b]Limited to central portion of channel above horizontal section of bed.

was used as the characteristic velocity throughout this study (Table 1).

[8] The log specimens were mounted on a test stand consisting of a powered vertical actuator supported between a concrete deadman buried in the channel bed and the overhead instrument bridge (Figure 1). The load cell incorporated a dual circuitry of differential strain gauge bridges that enabled simultaneous monitoring of the horizontal and vertical instantaneous forces acting perpendicularly to the log. The strains detected by the load cell were acquired with a strain indicator and recorder at a rate of 1 Hz and downloaded to a portable computer. The test stand allowed the log to be placed at various fixed elevations above the bed and at various angles to the approach flow. In all cases, contact between the log and the channel boundary was avoided to eliminate the influence of reaction forces. Additional details regarding experimental methods are provided by *Alonso et al.* [2005, 2009].

2.2. Cylindrical LW

[9] The 2004 tests were conducted with a simulated log (a PVC pipe) and quasi-cylindrical (unbranched), freshly cut hackberry (*Celtis occidentalis*) and oak (*Quercus sp.*) logs collected in the Stillwater area. For testing, each log was bolted to a load cell attached to the sliding carriage of the vertical actuator, and controls were provided to adjust the elevation and log yaw angle as needed (Figure 1). The yaw angle is defined as the angle between the incident flow velocity and the direction normal to the log's longitudinal axis (e.g., a yaw angle = 0° indicates that the log is perpendicular to flow, while yaw = 90° indicates that the log is parallel to flow; note that the yaw angle = 90° + orientation angle as defined by *Wohl et al.* [2010]). The load cell was covered with either PVC or bark linings to render a log piece of uniform diameter with an effective length of 1.80 m, slightly shorter than the 2 m length minimum often used to define LW in rivers. The stand was installed on the right descending bank toe such that the log spanned the entire width of the bed (Figure 1).

[10] As a comparative measure of the roughness of the evaluated logs, a roughness index was introduced and defined as: $I_k = (\varepsilon/\lambda)(p/P)$, where ε is the average roughness element height, λ is the average circumferential spacing between centers of consecutive roughness elements, and p is the portion of the log's total circumferential perimeter, P, that is occupied by roughness elements (Figure 2). This index was evaluated by taking averages over 8 cm long rough-log samples, and it approaches the correct limit for smooth cylinders. The parameters of the tested cylindrical logs are summarized in Table 2 along with values for tested cylinders reported in the literature. Here D and L are the log diameter and length, respectively, $Fr_l = \overline{U}_d/(gD)^{1/2}$ is the log Froude number, and $Re_l = D\overline{U}_d/\nu$ is the log Reynolds number. The denominator of the Reynolds number, ν, is the kinematic viscosity of water. The log Reynolds number reflects the influence of turbulence on the boundary layer development and separation around the log surface and associated vortex shedding on drag and lift forces. Similarly, the log Froude number measures the impact of standing surface waves on drag. These hydrodynamic dependencies are discussed in more detail by *Alonso* [2004].

2.3. Branched LW

[11] The 2005 tests involved noncylindrical LW specimens from hackberry trees and included a two-branched log, a four-branched log, and a root wad identified here as "short branches," "long branches," and "root wad," respectively (Figure 3). Logs were freshly harvested from the Stillwater area. All logs were positioned so that no portion of the test specimen was allowed to touch the channel boundary. Steady flow forces were measured for a series of yaw angles ranging from 0° to 90°. Logs were mounted on the test stand and rotated in the flow with branches upstream. Effects of yawing were amplified since naturally occurring LW is most frequently oriented with branches downstream [*Gippel et al.*, 1996; *Webb and Erskine*, 2005], a more streamlined configuration. The flow was stopped

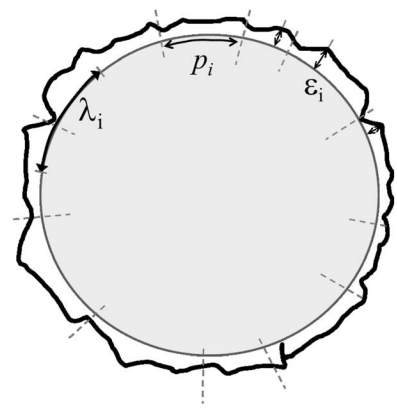

Figure 2. Definition of log roughness index. The log perimeter P is visually separated into sectors of length p_i, as depicted by the dashed line segments. The sectors can be either contiguous or separated by spaces, thus satisfying the condition $p = \sum_i p_i \leq P$. The roughness height ε_i associated with each sector is the maximum for that sector, and the length of the peripheral arc extended between the centers of any two contiguous bark sectors is represented by λ_i. The log roughness index is given by $I_k = (\varepsilon/\lambda)(p/P)$, where ε and λ are averages of ε_i and λ_i.

Table 2. Summary of Cylindrical Large-Wood and Test Cylinder Characteristics[a]

Cylinder	Diameter D (m)	Length L (m)	Roughness I_k	L/D	Fr_l	Re_l	Source
Hackberry	0.226	1.80	0.12	7.96	0.83	2.78×10^5	This study
Oak	0.229	1.80	0.46	7.86	0.82	2.82×10^5	This study
PVC	0.219	1.80	0	8.22	0.84	2.69×10^5	This study
PVC	0.0484	0.125–0.50	0	2.6–20.7	0.35–0.63	$2.18–2.90 \times 10^4$	*Gippel et al.* [1992]
Aluminum	0.019	0.61	0	32.1	n/a	4.50×10^4	*Bearman and Zdravkovich* [1978]
Steel	0.216	1.83	0	8.47	n/a	1.50×10^5	*Knoblock and Troller* [1935]
Steel	0.216	1.83	0	8.47	n/a	3.50×10^5	*Knoblock and Troller* [1935]
Aluminum	0.019	0.150	0	7.89	0.50	4.00×10^3	*Wallerstein et al.* [2002]

[a]Here n/a indicates not applicable.

after each series of yaw angle tests, the channel was drained, and the log was dismounted and rotated 90° around its axis and remounted to positions designated as rotation 1, 2, and 3. The channel flow was restored to the prescribed rate, and another series of measurements at varied yaw angles obtained. The projected area, a_θ, is defined as the log's wetted projected area on a plane perpendicular to the upstream flow direction with the log positioned at a yaw angle θ. For instance, in the case of cylindrical logs set normal to the upstream flow, $\theta = 0$ and $a_\theta = DL\cos\theta = DL$. In the case of branched LW, a_θ was determined for all log orientations (yaw angles and rotations) by digitizing photos collected after each log repositioning. The corresponding flow blockage ratio was evaluated as $B = a_\theta/A$. The projected areas and blockage ratios for all three logs and rotations are listed in Table 3 as a function of log yaw.

3. Evaluation of Hydrodynamic Loading

[12] The driving force acting on stream-borne, submerged, quasi-cylindrical logs can be expressed, in general, as [*Alonso*, 2004]:

$$\text{Driving Force} = \text{Streamwise Drag} + \text{Crosscurrent Lift} + \text{Buoyancy} + \text{Inertia} + \text{Reactions at contact points between log and streambed.} \quad (1)$$

[13] Other than for cases of stationary cylinders in unbounded uniform flows or subjected to harmonic waves, there is no general proof that these terms can be treated as additive [*Sarpkaya and Isaacson*, 1981]. Hence, application of equation (1) to more general configurations is justified on practical grounds only.

[14] By restricting the analysis to logs normal to the driving flow, equation (1) can be integrated over the log's length. If we relax the requirement that logs lie normal to the driving flow by using the area of the submerged body projected in the streamwise direction for computing drag force, solving for the horizontal and vertical components for the time mean drag and lift coefficients yields [*Alonso et al.*, 2005]

$$C_D = \frac{2g\overline{F}_H}{\gamma_w a_\theta \overline{U}_d^2} \quad (2)$$

$$C_L = \frac{2g[\overline{F}_V - \forall(\gamma_w - \gamma_l)]}{\gamma_w a_\theta \overline{U}_d^2} \quad (3)$$

where C_D and C_L are the drag and lift coefficients, g is the gravitational acceleration, $\overline{F}_H$ and $\overline{F}_V$ are the time mean values of the horizontal and vertical force components, respectively; a_θ is the cross-sectional area of the LW projected in the streamwise direction (i.e., $a_\theta = DL\cos\theta$ for cylinders), $\forall$ is the log volume, and γ_l and γ_w are the LW and water specific weight, respectively. $\overline{F}_H$ is acting in the direction parallel to $\overline{U}d$ (streamwise). It is noted that the second term on the right hand side of equation (3) represents the buoyant force. This force was evaluated for our tests by measuring the dry and submerged weight of each log prior to the runs. Since our apparatus measured the horizontal force acting perpendicularly to the log, $\overline{F}_n = \overline{F}_H\cos\theta$, we actually computed drag coefficients using a slightly modified form of equation (2):

$$C_D = \frac{2g\overline{F}_n}{\gamma_w a_\theta \overline{U}_d^2 \cos\theta} \quad (4)$$

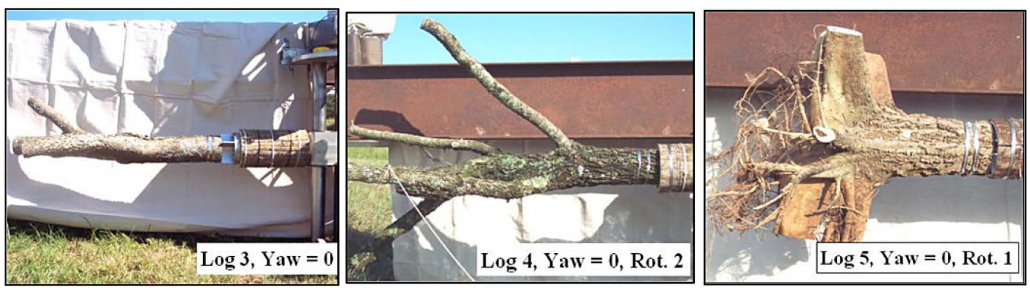

Figure 3. Branched logs and root wad mounted on test stand. Log 3, short branches; log 4, long branches; log 5, root wad.

Table 3. Projected Areas (m^2) and Blockage Ratios of Tested Branched LW

LW Specimen	Rotation	Yaw 0°	Yaw 45°	Yaw 60°
Short branches	Projected area	0.36	0.18	0.15
	Blockage ratio	0.11	0.06	0.05
Long branches	1	0.45	0.28	0.23
	2	0.47	0.34	0.26
	3	0.53	0.32	0.21
	Average projected area	0.48	0.31	0.23
	Average blockage ratio	0.15	0.10	0.07
Root wad	1	0.42	0.49	0.51
	2	0.47	0.34	0.32
	Average projected area	0.44	0.41	0.42
	Average blockage ratio	0.14	0.13	0.14

[15] Similarly, substituting $\overline{F}_L = \overline{F}_V - \forall(\gamma_w - \gamma_l)$ in equation (3) yields the corresponding lift coefficient:

$$C_L = \frac{2g\overline{F}_L}{\gamma_w a_\theta \overline{U}_d^2} \tag{5}$$

where F_H is the measured time mean net lift force.

3.1. Effect of Flow Blockage

[16] It should be noted that equations (2) and (3) yield apparent coefficients representative of horizontal and vertical loadings governed by the overall complexity of the flow pattern past the log. However, for comparison to measurements by others (as well as for design), it is useful to specify drag and lift coefficients that would reflect forces exerted by steady, uniform, infinite flows having the same yaw angle and approaching velocities, and free from interference from solid boundaries. *Gippel et al.* [1992] showed that channel boundary interference on drag of cylinders at zero yaw can be accounted for by

$$C_D = C_D^\infty (1 - B)^{-\beta} \tag{6}$$

where C_D^∞ represents the drag coefficient in the absence of solid boundary interference and the exponent β ranges from 1.35 to 3.00. A value for the exponent $\beta = 2.0$ was reported by *Gippel et al.* [1992] for model LW at middepth in a laboratory flume with bulk flow Froude number = 0.35, close to the range of Froude numbers that occurred in this study (0.26–0.43, Table 1). *Shields and Gippel* [1995] suggested using $\beta = 2.0$ for LW in natural rivers. This β value was adopted for adjustment of drag coefficients C_D to obtain the C_D^∞ values presented herein. A similar approach was considered for lift coefficients, but as noted below, C_L displayed no systematic variation with blockage ratio.

3.2. Drag Increase Due To Standing Surface Waves

[17] Herein we define the vertical location of LW as shown in Figure 4: G is the gap between the log and the bed, and z represents the distance from the LW axis to the free surface. Streamwise drag increases sharply whenever the free surface approaches the upper side of the log (Figure 5). This increase is attributed to the formation of surface deformations also known as standing waves, and it

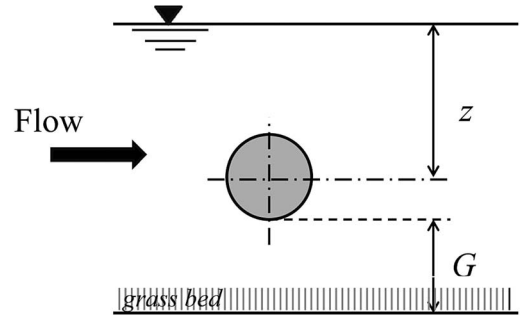

Figure 4. Definition of log position variables.

is referred to as wave drag. *Lamb* [1945] presented the first analysis of this phenomenon for the case of a two-dimensional, circular, stationary cylinder beneath the free surface of a steady, uniform, potential flow. He arrived at an expression for the wave drag force per unit length of cylinder that was rewritten by *Alonso* [2004] to yield the following expression for the wave drag coefficient, C_w:

$$C_w = \frac{\pi^2}{32} Fr_l^{-6} \exp[-(z/D)/2Fr_l^2] \tag{7}$$

[18] Equation (7) states that wave drag increases exponentially as submergence, z, decreases, and at any given depth decreases rapidly as Fr_l approaches 0 or when $Fr_l >> 1$ but goes through a maximum at intermediate Froude number values. Although this expression was derived for potential (inviscid) flow, the flume experiments reported by *Sheridan et al.* [1997] and related commentary by *Alonso* [2005] support the practical usefulness of the formula as well as its predicted functional behavior. The flume experiments conducted by *Wallerstein et al.* [2002] illustrated a similar dependence of the wave drag on log Froude number and submergence for smooth cylinders of finite length. These investigators evaluated the wave drag coefficient as the difference between the measured total drag coefficient, C_D, and the drag coefficient for cylinders submerged in deep flows, $C_{D_{z\max}}$, namely,

$$C_w = C_D - C_{D_{z\max}} \tag{8}$$

Figure 5. Testing PVC log showing standing wave that formed when water surface was near the top of the log.

[19] Equation (8) was used in this study to quantify wave drag, but it should be noted that its applicability is justified on practical grounds only.

3.3. Effect of Orientation

[20] As a log is turned into the flow, a significant flow component develops in the log's longitudinal direction and accentuates the three dimensionality of the flow in the near wake region [*Bursnall and Loftin* 1951; *Matsumoto et al.*, 1990; *Hoftyzer and Dragomirescu*, 2010]. To deal with this complexity, *Hoerner* [1965] invoked the "independence principle" assuming that the normal pressure forces are independent of the tangential flow component. Defining $\overline{U}_n = \overline{U}_d \cos\theta$ (Figure 6) and then using equation (2), the drag (horizontal) force acting on a cylindrical log is given by

$$\overline{F}_H = C_{D_0} a_\theta \frac{\gamma_w \overline{U}_n^2}{2g} = C_{D_0} a_\theta \frac{\gamma_w \overline{U}_d^2}{2g} \cos^2\theta, \tag{9}$$

[21] Where C_{D_0} is the drag coefficient for a cylinder placed normal to the flow (yaw angle = 0). By combining equations (2) and (9) we obtain

$$C_D = C_{D_0} \cos^2\theta. \tag{10}$$

[22] Equation (10) is known as Hoerner's rule. Clearly, this relation holds only for infinitely long cylinders that do not produce an end effect when rotated. Its utility for cylinders of finite length is limited to smaller yaw angles since such cylinders project a blunt face to the flow as yaw approaches 90°, resulting in a sharp increase in drag [*Gippel et al.*, 1992] while equation (10) suggests drag vanishes as yaw approaches 90°.

[23] In the case of branched LW, it is important to note that the resultant of the hydrodynamic forces acting on the branches and trunks is a randomly directed vector not likely to be coplanar in most instances with the longitudinal axis of the strain gauge cell. This resultant can in turn be replaced by a coaxial torque (not detected by the strain gauge cell), and a parallel force intersecting the cell longitudinal axis.

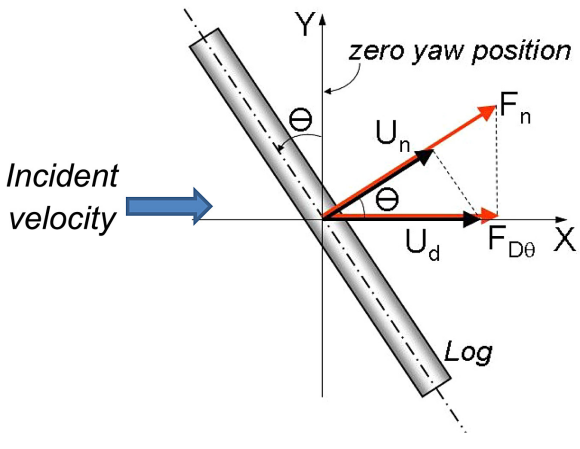

Figure 6. Definition sketch of velocity and force components acting on a yawed log lying on the X-Y horizontal plane.

This 3-D force can in turn be decomposed into coaxial, lift, and horizontal components, with the last two components measured directly by the cell, and the horizontal component equivalent to the force F_n depicted in Figure 6. Notwithstanding the fact that the "independence principle" is irrelevant when it comes to branched LW, equation (10) can still be used to evaluate the streamwise drag coefficient when the yaw angle <90°.

4. Results and Discussion

4.1. Cylindrical Logs, Steady Flow

4.1.1. Blockage Effects

[24] Drag coefficients were directly related to the blockage ratio, B, as indicated by equation (6). Figure 7 compares our drag coefficients for cylindrical LW placed normal to flow with data obtained in a water tunnel by *Shaw* [1971], data from laboratory flume runs reported by *Ramamurthy and Ng* [1973], data from a laboratory flume by *Gippel et al.* [1992, 1996], and equation (6). This plot exhibits considerable scatter, much of which is explained by the variation in geometry of the tested bodies and flow geometry. Lift coefficients displayed no systematic variation with blockage ratio. Over the full range of conditions tested ($0 <$ yaw < 75, $0.28 < G/D < 2.93$), C_D^∞ for cylindrical LW varied from −0.05 to 1.29, and C_L varied from −0.88 to 0.52. The negative drag value occurred in only one run, the one with the hackberry log placed at a yaw angle of 75° with a G/D of 1.61. Evidently this configuration resulted in turbulent eddies with significant upstream flow vectors.

4.1.2. Distance From Bed

[25] The tested logs had slenderness close to $L/D = 8$, and the log Reynolds numbers fell in the range where the drag of cylinders submerged in unbounded flows varies with Re_l and log roughness [*Alonso*, 2004; *Tanaka et al.*, 2011]. For logs perpendicular to the approach flow (yaw = 0), C_D^∞ varied from 0.58 to 1.29, increased with the gap ratio G/D, and varied inversely with log roughness (Figure 8). Measured drag coefficient values were comparable to values computed by *Alonso* [2004] using pressure distributions around a smooth cylinder placed at various heights above a smooth floor and perpendicular to the airstream in a wind tunnel reported by *Bearman and Zdravkovich* [1978]. For the wind tunnel case, drag increased from a minimum for cylinder location near the floor up to a nearly constant value for gap ratios $G/D > 1.0$. In contrast, the PVC drag coefficients did not vary much until $G/D > 2$ and then increased as the gap increased, while the hackberry and oak coefficients increased continuously with increasing gap. Values of C_D at middepth ($G/D \sim 1.3$) were similar to those reported by *Tanaka et al.* [2011] for cylindrical logs in a wind tunnel. With the $G/D \sim 2$ and the upper surface of the log about 0.10 m below the free surface ($z/D \sim 1$), the PVC drag coefficient attained a value (0.85) close to those predicted for smooth cylinders with $L/D = 8$ by an empirical formula presented by *Gippel et al.* [1992]. Since C_D^∞ increases asymptotically with increasing L/D because of "leakage" of flow around the ends of the cylinder at lower L/D [*Gippel et al.*, 1992; *Alonso*, 2004; *Tanaka et al.*, 2011], it is reasonable that values depicted in Figure 8 are

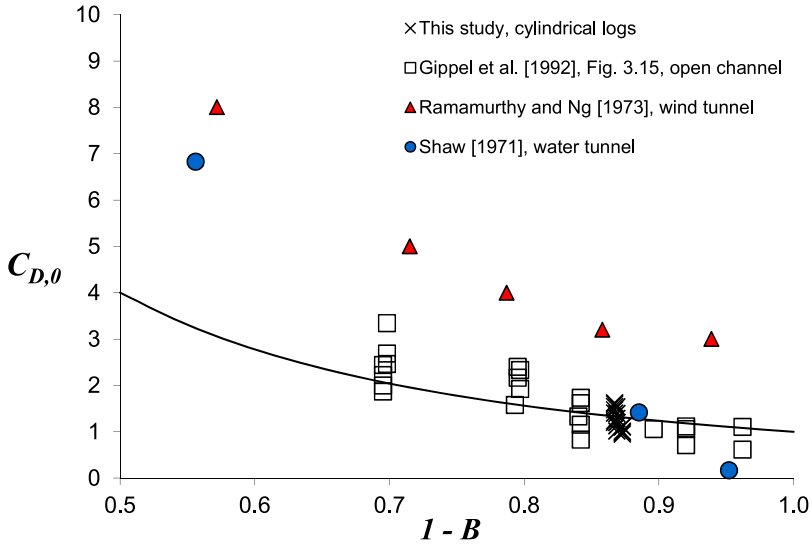

Figure 7. Relationship between measured drag coefficient and blockage for yaw = 0. Data from this study are for large wood (LW) placed at middepth and characteristic velocity, $\overline{U}_d = 1.23$ m s^{-1}. Solid curve is the relation suggested by *Gippel et al.* [1992] for cylinders at middepth in an open channel with a Froude number of 0.35. This relation is given by equation (6) with $\beta = 2.0$.

somewhat smaller than the one ($C_D^\infty = 1.14 \pm 0.17$) reported by *Manga and Kirchner* [2000] for a cylindrical log with $L/D = 38.4$ suspended in a 0.29 m deep gravel bed stream. Our values are also somewhat smaller than those measured by others ($1.05 < C_D^\infty < 1.20$) for cylinders with "infinite" L/D at Re_l values comparable to the ones that occurred in our experiments [*Alonso*, 2004]. It should be noted that the higher asymptotic value displayed by the wind tunnel data relative to the PVC data in Figure 8 is due to scaling differences introduced by the incongruence of velocity distributions in the channel and wind tunnel tests.

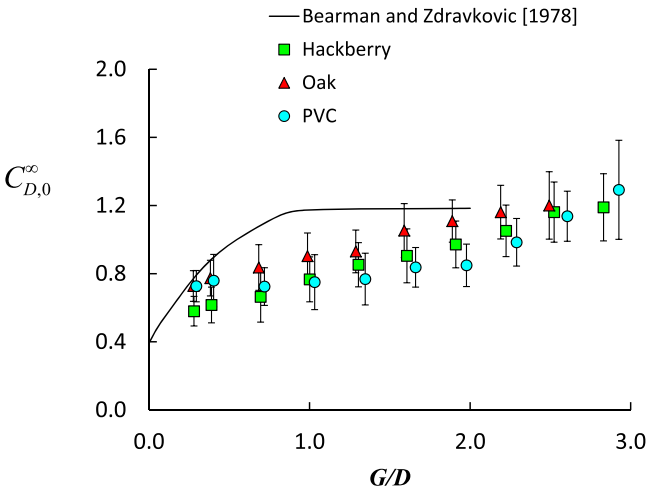

Figure 8. Mean drag coefficients for logs and cylinders oriented perpendicular to steady incident flow versus dimensionless distance above bed. Data sources in legend are defined in Table 2. Vertical error bars are ±1 standard deviation of drag coefficients computed from the 1 Hz load cell data.

The fact that there is no leveling off of the hackberry and oak data at intermediate G/D suggests the zones influenced by the proximity of the bed and of the free surface overlapped. The log coefficients did not decrease as rapidly toward the bed as the wind tunnel data did, which may be explained by the presence of the grass lining in the test channel. The smallest clearance, G, between the logs and the bed surface was about 0.06 m, and the grass may have disturbed the flow under the log enough to cause an upstream shift of the separation point and an enlargement of the wake. Temporal variations in drag forces detected by our 1 Hz load cell produced standard deviations in drag coefficients that were <0.2, and coefficients of variation that were between 12% and 22% for the range of G/D values tested for logs placed normal to the incident flow.

[26] For logs lying close to the bed, flow past the log induces pressure gradients on the bed resulting in separation and inclination of the flow approaching the log. This not only influences drag near the bed as shown above but also leads to a lift component of the total mean force on the cylinder acting away from the bed. Figure 9 shows the effect of bed proximity on the lift coefficients of the tested logs and compares these coefficients to values reported by *Knoblock and Troller* [1935]. They measured lift on a smooth cylinder suspended in a wind tunnel with its axis parallel to a wall and normal to the flow direction for Reynolds numbers in the range $1.5 \times 10^5 < Re_l < 3.5 \times 10^5$. The log and wind tunnel data plotted in Figure 9 follow parallel trends, but diverge for $G/D < 0.7$, lift coefficients decrease exponentially with increasing G/D. This departure is also attributable to incongruent velocity distributions. The log data display a small but apparent drop in lift due to roughness that is most likely associated with the upstream shift of the separation points in the log wake [*Bearman and Zdravkovich*, 1978]. Log data becomes more variable and negative lift occurs as G/D increases beyond 1.5, indicating free surface effects as noted for drag in the discussion of

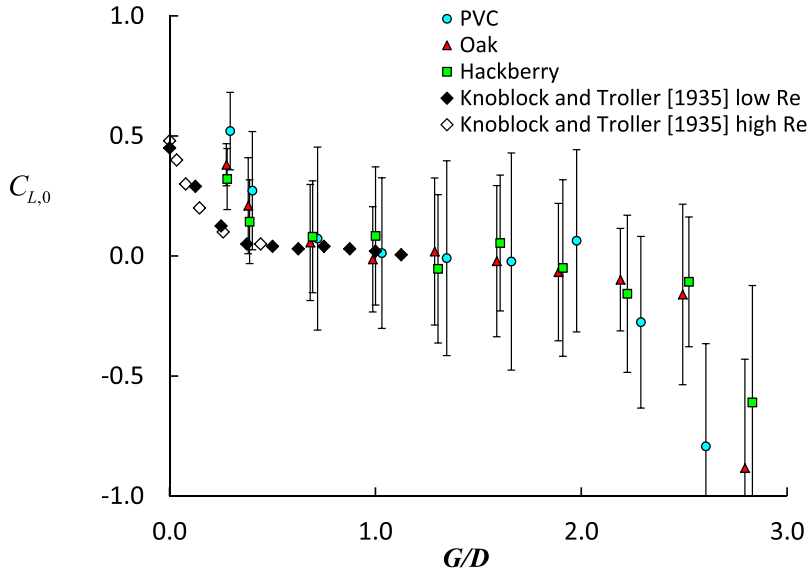

Figure 9. Variation of lift coefficient for cylindrical LW placed normal to flow (yaw = 0) with roughness and submergence. Data sources in legend are defined in Table 2. Vertical error bars are ±1 standard deviation of lift coefficients computed from the 1 Hz load cell data.

Figure 8 above. Standard deviations of lift coefficients were generally <0.5 for $G/D < 1.30$, and were most variable as logs approached the free surface ($G/D > 2.5$).

4.1.3. Relative Submergence and Wave Drag

[27] Largest drag coefficients were associated with low z/D when logs were barely overtopped by flow (Figure 8, $G/D = 3.0$) triggering formation of standing waves. Equation (8) was applied to the data for logs normal to flow (yaw = 0) using the drag coefficients measured at middepth ($G/D = 1.30$, shown as X-symbols in Figure 7) for $C_{D_{z\max}}$. The results are compared in Figure 10 with similar data obtained by *Wallerstein et al.* [2002] for a smooth cylinder with $L/D = 7.9$, and the wave drag coefficient predicted by equation (7) using the average log Froude number for the cylindrical log tests. When the undisturbed free surface was within two log diameters of the top of the log, drag increased and became more variable as z/D decreased because of the onset of wave drag (Figure 10). The data parallel the exponential increase in C_W predicted by equation (7) for $z/D < 1.0$, although the observed wave drag coefficients are considerably lower than predicted by equation (7). Increased log roughness led to a small systematic decrease in wave drag (Figure 10), most likely caused by a shift of the separation layer emanating from the top of the log [*Sheridan et al.*, 1997; *Alonso*, 2005].

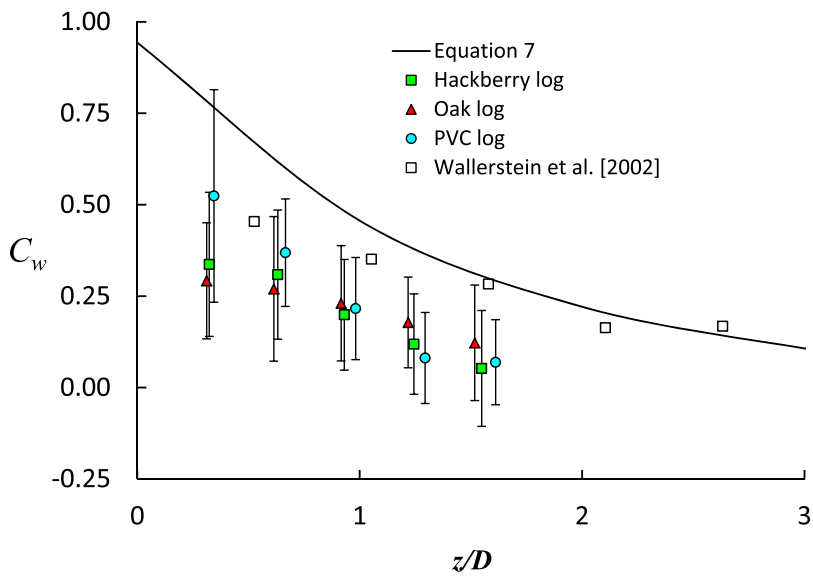

Figure 10. Variation of wave drag with log roughness and submergence. Data sources in legend are described in Table 2. Vertical error bars are ±1 standard deviation of drag coefficients computed from the 1 Hz load cell data.

4.1.4. Orientation

[28] Drag coefficients were inversely related to yaw angle. Figure 11 compares equation (10) with similar values computed from data measured with the logs positioned near middepth and with data reported by *Gippel et al.* [1992] (see Table 2). All measured drag coefficients in Figure 11 have been adjusted for blockage effects using equation (6). In general, the drag coefficients obtained here are in agreement with those reported by *Gippel et al.* [1992] for yaw angles between 0° and 70°. Trends for experimental data followed Hoerner's rule for yaw angles between 15° and 75°, but C_D^∞ magnitudes were greater since Hoerner's rule does not account for end effects of cylinders of finite length. In contrast to equation (10), the *Gippel et al.* [1992] drag coefficients rise quite sharply for yaw >75° as the result of three distinct additive mechanisms: (1) the shear layer that separates from the cylinder leading edge giving rise to a significant forebody drag, (2) the surrounding flow reattaches to the cylinder side around three log diameters from the leading edge, and from this point on a turbulent boundary layer develops adding skin drag, and (3) as the boundary layer grows, the cylinder wake widens contributing an additional form drag which can be considerable in the subcritical cylinder Reynolds number range [*Higuchi et al.*, 2005]. It should be noted that these mechanisms and associated horizontal forces not acting normal to the log were not detectable by our measuring setup. Coefficients of variation for the other orientation angles tested ranged from 15 to 34%, while C.V. for the drag coefficients for $\theta = 75°$ were 37%, 59% and 172%, for PVC, oak, and hackberry logs, respectively.

4.2. Cylindrical Logs, Unsteady Flow

[29] Data presented above were from runs when flow rates were held steady. Natural streams experience unsteady flows which give rise to extreme (design) conditions. A limited number of test runs were conducted with unsteady flows, and data from two of these runs are provided in Figure 12, which illustrates the combined effect of vortex shedding and standing surface waves on the instantaneous drag and lift experienced by a cylindrical log subjected to a rising and falling hydrograph. The data in Figure 12 are from runs with logs placed perpendicular to the flow (yaw = 0) with their inverts 0.066 m ($G/D = 0.30$) above the bed, a configuration similar to that observed for naturally occurring logs in small streams with sand beds [*Wallerstein et al.*, 1997]. Drag forces increase sharply as flow stage increases and reach their maximum shortly after flow overtops the log because of the onset of a standing surface wave followed by a decrease toward the steady state value when the log becomes fully submerged. A similar, though much less marked rise and fall is observed in lift. As water flows over the log submerging its wake, both drag and lift develop high-frequency fluctuations created by vortices emitted by the log's wake. Generally, less variation occurred during receding limbs than the rising limbs. Steady state lift variations were greater for the smooth than for the moderately rough log while drag variations were slightly greater for the moderately rough log. The combined impact of surface-wave interaction and vortex shedding generated instantaneous excursions of drag about twice as large as the steady flow average, while lift maxima were up to 2.8 and 1.9 times the steady flow values for the PVC and Hackberry, respectively ($G/D \sim 0.3$, Figure 9). In small, flashy streams, the sum of applied forces on a given LW formation or structure is likely greatest early in a high-flow event when buoyant forces are maximized because of unsaturated wood and drag forces are elevated because of wave formation as the LW is just overtopped by rising waters. As an event proceeds, buoyancy will decline as wood becomes saturated and local scour should produce

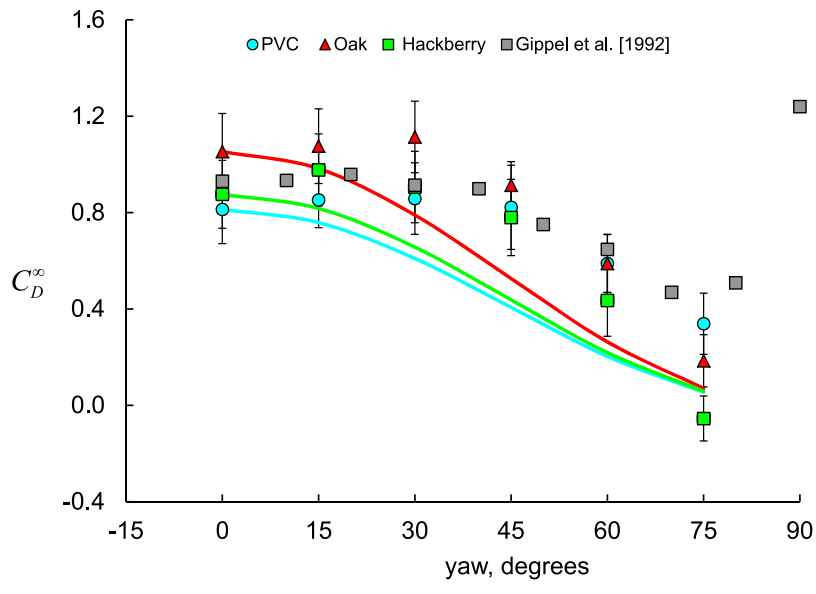

Figure 11. Variation of measured drag coefficients for cylindrical LW and PVC cylinders with yaw compared with Hoerner's rule (solid curves, equation (10)). A yaw = 0 implies the cylinder lies normal to the approach flow, while yaw = 90 implies the axis of the cylinder is parallel to the flow. Vertical error bars are ±1 standard deviation of drag coefficients computed from the 1 Hz load cell data.

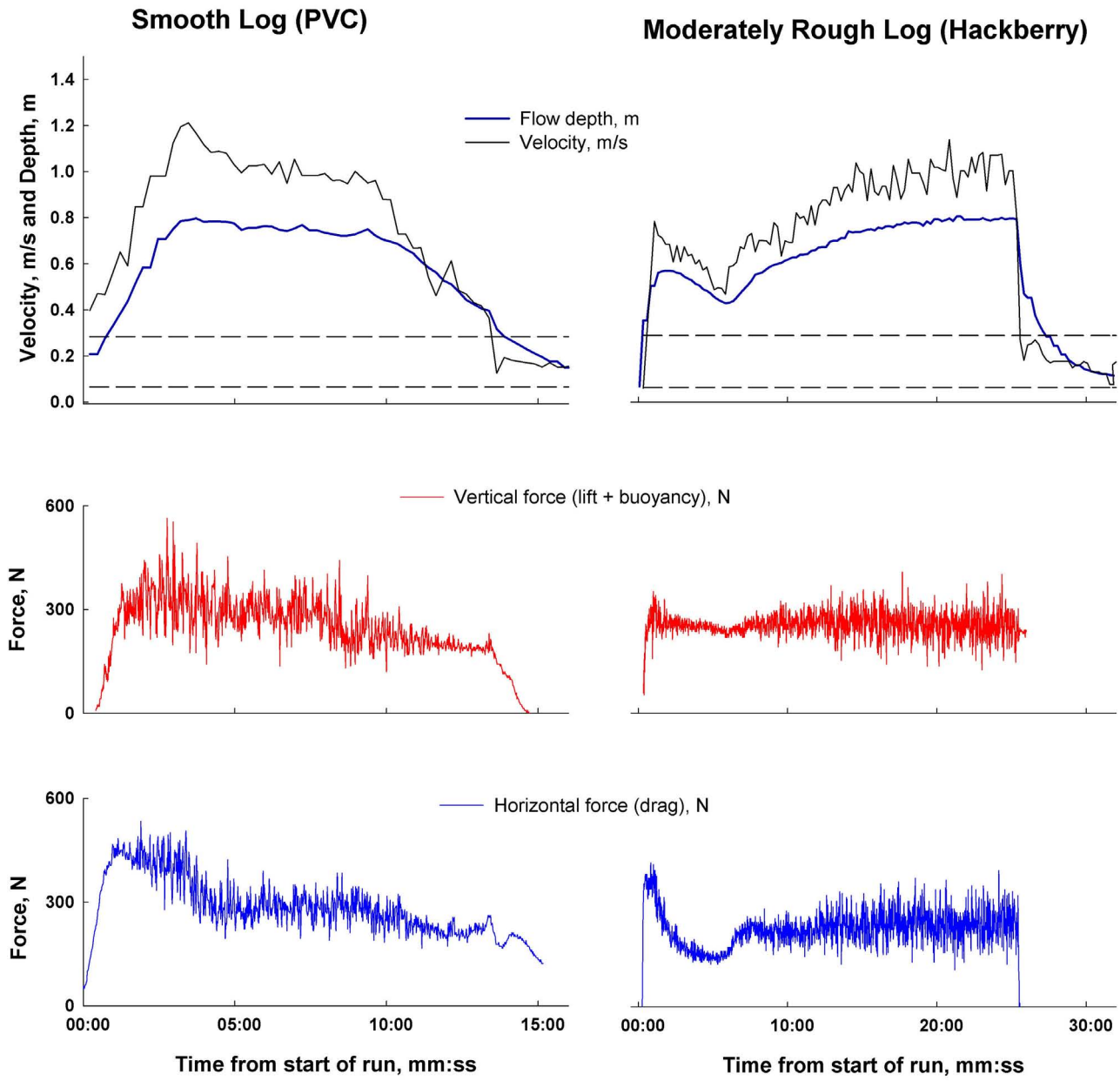

Figure 12. Flow depth, centerline velocity, and forces during unsteady flows with smooth and moderately rough cylindrical logs placed normal to flow direction, 0.066 m above the bed. Horizontal dashed lines in the top plots represent the location of the tops and bottoms of logs. Flow velocity is depth-averaged velocity measured at channel centerline. Vertical force is lift plus net buoyant force.

reductions in the near-field velocity and thus asymptotically decreasing drag forces [*Wallerstein et al.*, 2001].

4.3. Branched LW, Steady Flow

[30] Drag coefficients varied with incident velocity and yaw angle in a nonsystematic fashion (Figure 13), with generally higher C_D^∞ at the lower velocity, suggesting at least some branches may have been in the subcritical Re_l range at that flow condition [*Bursnall and Loftin*, 1951; *Alonso*, 2004, Figure 3]. Despite the higher values of drag coefficient at lower velocity, actual drag forces were greater at the higher velocity. Exploratory analyses of variance confirmed the impression gained from Figure 13: drag coefficient variation due to yaw was insignificant, while variation due to LW specimen was significant ($p < 0.001$). Furthermore, as LW complexity increased, average C_D^∞ values converged on those for blunt bodies (mean $C_D^\infty = 4.06$ for short branches, 1.68 for long branches, 0.91 for root wad). Similar findings were reported by *Gippel et al.* [1996] for small model LW of increasing complexity and in a review by *Mutz* [2003]. Measured C_D^∞ for noncylindrical LW at yaw = 0 fell between 0.98 and 5.14. This range differs significantly from the range of values reported for cylinders and blunt bodies; most likely reflecting the fact that most of the apparent drag is due to the bending moments exerted by the hydrodynamic forces acting on the branches. At larger

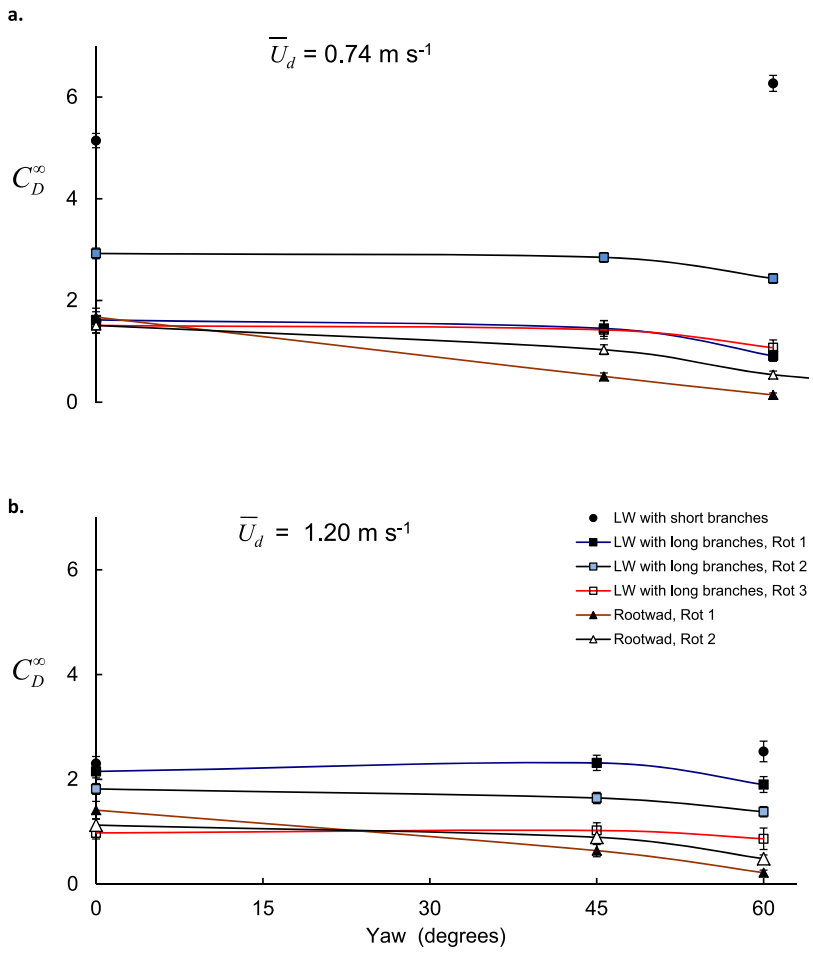

Figure 13. Drag coefficients for branched large wood in uniform, steady flows with characteristic velocities (a) $\overline{U}_d = 0.74$ m s^{-1} and (b) $\overline{U}_d = 1.20$ m s^{-1}. Vertical error bars are ± 1 standard deviation of drag coefficients computed from the 1 Hz load cell data.

yaw angles, drag coefficients tended to diverge, producing a range for C_D^∞ over the full range of yaw of 0.22 to 6.27, comparing favorably with values of 0.7 to 9.0 reported by *Manners et al.* [2007] for drag coefficients of natural LW formations. Measured values of C_D^∞ for the branched LW were also considerably influenced by the log rotation (Figure 13; note that rotations 2 and 3 for the short-branched log did not yield useful data because of instrument problems). On the other hand, drag coefficients for the root wad were less variable and displayed similarity with the standard drag-yaw relationships for blunt bodies within the 0°–45° range. Temporal variations within a given run were less for the branched LW than for the cylindrical LW, with standard deviations of C_D^∞ ranging from 0.04 to 0.20.

[31] Lift coefficients C_L for noncylindrical LW varied widely, reflecting vertical components of drag on angled branches and roots (Figure 14). Lift coefficients for LW placed normal to the flow ranged from -1.71 to 4.84, diverging as yaw angle increased, producing a range from -3.65 to 30.84 over the full range of tested yaw angles. Further, lift coefficient values were much more variable at the lower approach velocity (Figure 14). Again, this variation likely manifests the results of complex frontal geometries engaging the flow and phenomena unique to flows in the "drag crisis" range of Reynolds numbers for the lower velocity flows. Exploratory analyses of variance indicated that the effect of yaw angle was insignificant while effects of LW specimen were significant at $p = 0.027$. Temporal variability of lift coefficients was greater than for drag, with standard deviations ranging from 0.07 to 0.76. As for drag coefficients, C_L values became smaller as LW complexity increased, with a means of 10.56 for the short-branched specimen, 3.64 for the long-branched specimen and 3.04 for the root wad.

[32] Some of the variation in drag and lift coefficients depicted in Figures 13 and 14 is likely due to errors in measuring the projected area, a_θ, by digitizing the LW outlines on two-dimensional photographs. No attempt was made to correct for apparent changes in log dimensions due to varying distance from the camera. Inspection of the resulting projected areas indicates such errors were slight, and the issue of precise determination of projected area is mitigated in when dealing with actual LW formations and structures since branches and limbs often cluster closely together [*Gippel et al.*, 1992] and accrete organic debris and sediments [*Manners et al.*, 2007], allowing use of simple solid geometries (e.g., wedge or prism) for determining frontal areas.

4.4. Branched LW, Unsteady Flow

[33] As for cylindrical logs, a limited number of test runs were conducted subjecting branched LW placed normal to

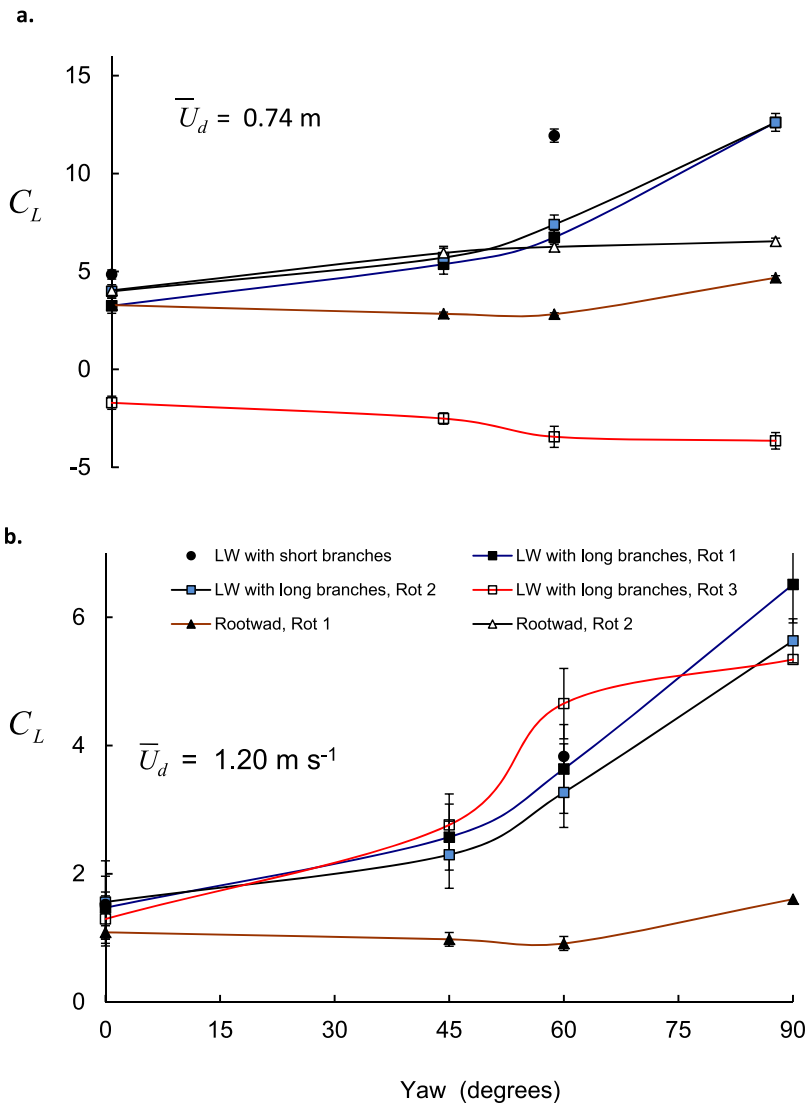

Figure 14.* Lift coefficients for branched large wood in uniform, steady flows with characteristic velocities (a) $\overline{U}_d = 0.74$ m s^{-1} and (b) $\overline{U}_d = 1.20$ m s^{-1}. The lift coefficient for the short-branched log at yaw = 90 in Figure 14a is 30.8 (off scale).

the channel to unsteady flows, and time series for rising limbs of two typical events are depicted in Figure 15. Velocity data were not obtained for these runs. Lift forces displayed much wider variation for the log with long branches than for the blunt, nearly solid root wad (Figure 3), reflecting interaction of wakes created by the main trunk and individual branches of the branched log. For both LW specimens, the lift forces increased as flow stage increased and then fluctuated about a mean condition, with maxima that were more than two times greater than the steady flow mean values for the branched log and roughly equal to the steady flow mean for the root wad. Drag forces for the branched log increased smoothly to a mean condition at peak flow in contrast to the drag curve for cylindrical logs (Figure 12), perhaps reflecting the interactions of wakes produced by the main stem and branches. Maximum measured drag forces were 1.3 times (branched log) and 1.4 times (root wad) the mean values measured for steady flows at yaw = 0.

5. Comparison With Work by Others

[34] Comparison of our observations with two other studies involving prototype scale measurements of drag on LW in streams is presented in Table 4. No other studies containing field measurements of LW drag were found, although there are numerous laboratory flume studies. Using a torque wrench and a handheld test stand, *Hygelund and Manga* [2003] measured torque created by drag on PVC cylinders held parallel to the bed of shallow, spring-fed gravel bed rivers. *Manners et al.* [2007] measured velocities at the perimeter of control volumes around bank deflector-type LW formations in a cobble and boulder bed river. LW formation porosity to flow was manipulated by first covering the LW formation with plastic, removing the plastic, and then removing various amounts of LW, sediment and debris until only key members remained. The other studies did not report

*Figure 14 and its caption have been replaced here. The article as originally published appears in the HTML.

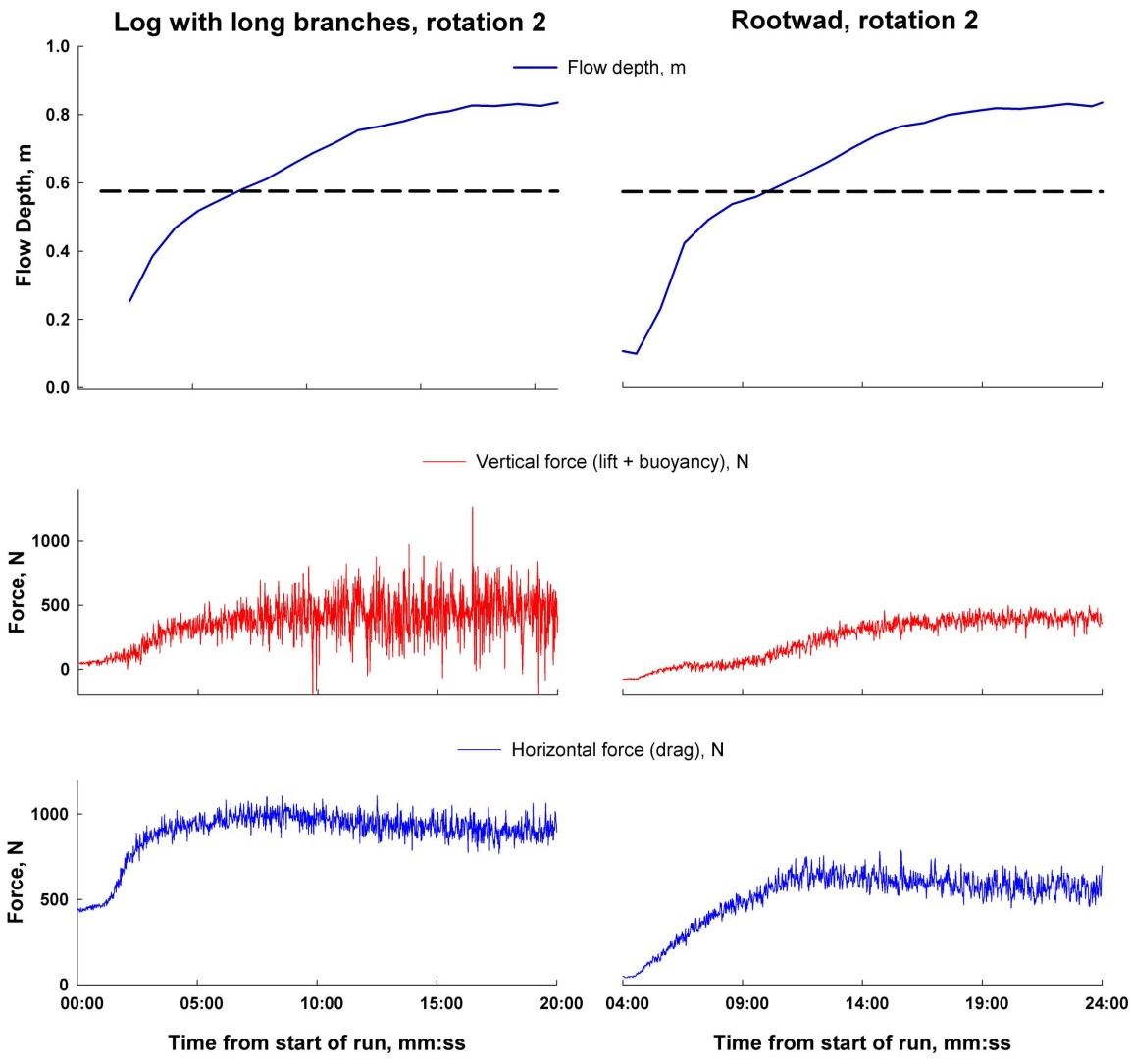

Figure 15. Flow depth and forces during unsteady flows for LW with long branches and root wad placed normal to flow direction. Horizontal dashed lines in the top plots represent the location of the tops of log stems. Vertical force is lift plus net buoyant force. Velocity data were not obtained for these runs; for both cases, the bulk flow velocity (Q/A) at peak is 1.06 m s^{-1}.

lift or temporal variations in drag and lift. Differences between our findings and those of *Hygelund and Manga* [2003] regarding the effect of blockage may arise because they defined the blockage ratio as the ratio of cylinder diameter to flow depth. Since their channels were very wide, blockage ratios computed using our definition would have been very small. *Hygelund and Manga* [2003] suggested that the difference between their findings and those of *Gippel et al.* [1992] regarding the sensitivity of drag to log orientation was due to incongruent velocity profiles. There were strong vertical velocity gradients in the shallow, gravel bed streams used by *Hygelund and Manga* [2003].

6. Application

[35] Structures made from LW are widely used for stream habitat rehabilitation and enhancement, but often fail prematurely [*Shields et al.*, 2008b; *Southerland and Reckendorf*, 2010]. If large wood structures (LWS) placed in streams are to remain long enough to perform their intended functions, they usually must be restrained using ballast (e.g., cobbles and boulders), anchors, or by keying members of the LWS into bank soils. Prediction of flow forces on LW are needed for design of restraint systems. Similar computations are needed for transport analyses for unanchored LW. Measurement of lift and drag forces on noncylindrical LW indicates that greatest forces occur for simple configurations (only a few large branches), and that lift and drag coefficients approach those for blunt bodies as branch size declines and branch density increases. New LW formations [*Manners et al.*, 2007] and LW structures [*Shields et al.*, 2004] accrete large volumes of sediment, wood and other organic debris. As LW decays, smaller branches disintegrate first [*Spanhoff and Meyer*, 2004], simplifying the LW matrix and creating conditions conducive to higher-flow forces and thus wood entrainment and structural failure [*Shields et al.*, 2004].

[36] Uncertainty associated with computation of the applied forces may be addressed during design by using safety factors. However, since benefits of environmentally

Table 4. Comparison of Findings of This Study With Work by Others[a]

	Hygelund and Manga [2003]	*Manners et al.* [2007]	This Study
Setting	Two spring-fed rivers with near constant discharge	Regulated river with steady flow for several hours	Trapezoidal channel with controlled inflow
Bed	Gravel with median grain sizes of 3.5 and 16 mm	Cobbles and boulders, median grain sizes 100–280 mm	Grass
Depth (m)	0.40 and 0.48	1.0 to 1.7[b]	0.83 and 0.85
Top width (m)	Not given	40 to 60	5.7
Velocity (m s^{-1})	0.16 and 0.33	0.20 to 1.40	0.74 and 1.20
Large wood specimens	PVC cylinders with diameters 0.048 to 0.274 m	Natural bank deflector type LW formations	See Table 2 and Figure 3
Re_l	4×10^3 to 6×10^4	n/a	2.7×10^5 to 2.8×10^5
Range of C_D	1–3	0.7 to 9	0 to 6.3
Range of C_L	n/a	n/a	−3.6 to 31
Effect on C_D			
Blockage ratio B	No effect[c]	n/a	According to relation given by *Shields and Gippel* [1995]
Distance above bed	Increased with increasing distance above bed for $B < 0.3$	Removing part of debris may likely allowed flow between key member and bed, accounting for observed increase in C_D	Increased with increasing distance above bed, especially for rougher natural logs
Distance below surface	n/a	n/a	Wave drag varied inversely with distance below surface for submergence less than one log diameter
Orientation in horizontal plane ("yaw angle")	No effect	n/a	For cylinders, sharp decrease for yaw between 30° and 75°; no systematic variation for noncylindrical LW
Temporal variations	n/a	n/a	Instantaneous maxima were 2 to 3 times temporal means

[a]Here n/a indicates not reported.
[b]We estimated *Manners et al.*'s [2007] depth from channel cross-section plots.
[c]*Hygelund and Manga* [2003] computed blockage on the basis of the ratio of log diameter to flow depth rather than ratio of areas.

driven projects are often hard to quantify, excessively large safety factors that increase costs are undesirable. One approach for reducing uncertainty is to extrapolate drag and lift forces measured in laboratory flumes to naturally occurring scales. Measured drag and lift forces might be used to compute drag and lift coefficients using equations (2) and (3) and corresponding drag coefficients for unbounded flows might be derived using equation (6) and site geometry. The resulting value of C_D^∞ could be applied with design values for characteristic flow velocity and wood density to solve equations (2) and (3) for the design loads. Additional loads due to wave drag when flow just overtops the LW could be estimated using equation (7). Force values obviously depend on how closely the laboratory test configuration approximates the field configuration, but findings presented here suggest that appropriately scaled lab tests can reproduce field loadings. Forces on LW structures with complex geometries may be measured in laboratory flumes [*Ward et al.*, 2007].

[37] Uncertainty may also be addressed by subjecting the system of equations describing the loads on restraints to Monte Carlo analyses (MCA) wherein probability density functions for each key input variable are assumed on the basis of experience and reports of studies such as the one described here, and design loads are computed using a large number of randomly generated values for each variable. In lower velocity streams with LW that experiences episodic wetting and drying, the uncertainty in the specific gravity of LW may give rise to significant variation in buoyant forces, which increase relative to lift and drag as incident velocities decrease [*Shields et al.*, 2004; *Thevenet et al.*, 1998]. *Shields et al.* [2004] reported a range for in situ specific gravity of 0.30 to 1.39 for 93 wood samples with varying moisture content collected from LW along a Mississippi stream, but *Bilby et al.* [1999] reported continuously immersed LW experienced little change in density (except for the top ~20 mm) over 60 months. Following MCA, an appropriate design load may be selected on the basis of the frequency distribution for the load that must be resisted by restraints, and adjusted using appropriate values of safety factor. Analyses should take full account of the upper levels of lift and drag likely to occur during unsteady flows and because of turbulent fluctuations in steady flows. We found that maximum lift and drag forces during the rising limb of unsteady flows were about 2 to 3 times as great as steady flow temporal mean values.

7. Summary and Conclusions

[38] The preceding results hint strongly at the scalability of laboratory data to field-size logs, hence future data collection can take advantage of controlled laboratory experiments. The combined effect of buoyancy, drag, and lift forces acting on a cylindrical log is at a maximum when the log is oriented normal to the flow, and either resting on the bed or just barely submerged. The bark roughness of cylindrical logs has an opposite effect on lift (roughness increases lift) and wave drag (roughness reduces wave drag), and it has less significance than log proximity to the bed and the free surface. Time mean drag and lift coefficients of cylindrical logs are amenable to characterization by general functions depending on current velocity, log alignment and boundary proximity parameters. On the other hand, drag and lift coefficients for branched logs and root wads experience considerable variation with the geometry of a given specimen or LW formation but generally

trend toward values typical of blunt bodies as LW complexity increases. These findings underscore those of *Manners et al.* [2007], who commented (their paragraph [73]) on LW drag coefficients that "the relationship between single logs and complete debris jams is complex and nonlinear" and that "the number and size of pieces, as well as the arrangement of these pieces . . . can significantly affect the hydraulics . . . of individual debris jams." Temporal variations in lift and drag produce forces that are about 2 to 3 times as great as steady flow mean values. Additional work is needed to refine knowledge of LW behavior in nonlaboratory settings: forces associated with complex LW geometry, formations of LW (jams), interaction with sediment transport, scour and deposition, effects of impacts from bed load and floating LW, ice effects, unsteady phenomena, and effects of beaver activities.

[39] **Acknowledgments.** The authors are grateful to John Cox, Glenn Gray, John Milam, Tony Smith, John Stofleth, Mick Ursic, Darrel Temple, Greg Hanson, Kem Kadavy, Bobby Sappington, Ron Tejral, and Raymond Cox for their assistance during equipment fabrication, calibration, setup, and operational runs. Mary A. McCaskill assisted with manuscript preparation. Nick Wallerstein, Daniel Wren, Sean Bennett, J. R. Rigby, C. J. Gippel, the WRR Associate Editor, and two anonymous referees read an earlier version of this paper and made many helpful comments.

References

Alonso, C. V. (2004), Transport mechanics of stream-borne logs, in *Riparian Vegetation and Fluvial Geomorphology, Water Sci. Appl.*, S. J. Bennett and A. Simon, vol. 8, pp. 59–69, AGU, Washington, D. C.

Alonso, C. V. (2005), Discussion of "Hydrodynamic loading on river bridges," by S. Malavasi and A. Guadagnini, *J. Hydraul. Eng.*, *131*(7), 619–621.

Alonso, C. V., F. D. Shields, and D. M. Temple (2005), Experimental study of drag and lift forces on prototype scale models of large wood, paper presented at ASCE World Water and Environmental Resources Congress, Am. Soc. of Civ. Eng., Anchorage, Alaska.

Alonso, C. V., F. D. Shields, Jr., and D. M. Temple (2009), Dynamics of large wood: A prototype-scale flume experiment, paper presented at Water Engineering for a Sustainable Environment, 33rd Congress, Int. Assoc. for Hydro-Environ. Eng. and Res., Vancouver, B. C., Canada.

Assani, A., and F. Petit (1995), Log-jam effects on bed-load mobility from experiments conducted in a small gravel-bed forest ditch, *Catena*, *25*, 117–126, doi:10.1016/0341–8162(95)00004.

Bearman, P. W., and M. M. Zdravkovich (1978), Flow around a circular cylinder near a plane boundary, *J. Fluid Mech.*, *89*(1), 33–47.

Beebe, J. T. (2000), Flume studies of the effect of perpendicular log obstructions on flow patterns and bed topography, *Great Lakes Geogr.*, *7*(1), 9–25.

Benke, A. C., R. L. Henry III, D. M. Gillespie, and R. J. Hunter (1985), Importance of snag habitat for animal production in southeastern streams, *Fisheries*, *10*(5), 8–13.

Bilby, R. E., J. T. Heffner, B. R. Fransen, J. W. Ward, and P. A. Bisson (1999), Effects of immersion in water on deterioration of wood from five species of trees used for habitat enhancement projects, *North Am. J. Fish. Manage.*, *19*(3), 687–695.

Borg, D., I. Rutherford, and M. Stewardson (2007), The geomorphic and ecological effectiveness of habitat rehabilitation works: Continuous measurement of scour and fill around large logs in sand-bed streams, *Geomorphology*, *89*, 205–216.

Braudrick, C. A., and G. E. Grant (2000), When do logs move in rivers?, *Water Resour. Res.*, *36*(2), 83–571.

Braudrick, C. A., and G. E. Grant (2001), Transport and deposition of large woody debris in streams: A flume experiment, *Geomorphology*, *41*, 263–283.

Brooks, A. P., T. Howell, T. B. Abbe, and A. H. Arthington (2006), Confronting hysteresis: Wood based river rehabilitation in highly altered riverine landscapes of south-eastern Australia, *Geomorphology*, *79*, 395–422.

Bursnall, W. J., and L. K. Loftin (1951), Experimental investigation of the pressure distribution about a yawed circular cylinder in the critical Reynolds number range, *NACA Tech. Note*, *2463*, 34 pp.

Buxton, T. H. (2010), Modeling entrainment of waterlogged large wood in stream channels, *Water Resour. Res.*, *46*, W10537, doi:10.1029/2009WR008041.

Cherry, J., and R. L. Beschta (1989), Coarse woody debris and channel morphology: A flume study, *Water Resour. Bull.*, *25*(5), 1031–1036.

Cordova, J. M., E. J. Rosi-Marshall, A. M. Yamamuro, and G. A. Lamberti (2006), Quantity, controls and functions of large woody debris in midwestern USA streams, *River Res. Appl.*, *23*(1), 21–33.

Daniels, M. D., and B. L. Rhoads (2003), Influence of a large woody debris obstruction on three-dimensional flow structure in a meander bend, *Geomorphology*, *51*, 159–173.

D'Aoust, S. G., and R. G. Millar (2000), Stability of ballasted woody debris habitat structures, *J. Hydraul. Eng.*, *126*(11), 810–817.

Downs, P. W., and A. Simon (2001), Fluvial geomorphological analysis of the recruitment of large woody debris in the Yalobusha River network, central Mississippi, USA, *Geomorphology*, *37*, 65–91.

Erskine, W. D., A. C. Chalmers, and M. Townley-Jones (2010), The importance of sediment control for recovery in incised channels, *IAHS Publ.*, *337*, 211–219.

Fremier, A. K., J. I. Seo, and F. Nakamura (2010), Watershed controls on the export of large wood from stream corridors, *Geomorphology*, *177*(1–2), 33–43.

García, M. H., F. López, C. Dunn, and C. V. Alonso (2004), Flow, turbulence, and resistance in a flume with simulated vegetation, in *Riparian Vegetation and Fluvial Geomorphology, Water Sci. Appl.*, edited by S. J. Bennett and A. Simon, vol. 8, pp. 11–27, AGU, Washington, D. C.

Gippel, C. J. (1995), Environmental hydraulics of large woody debris in streams and rivers, *J. Environ. Eng.*, *121*, 388–395.

Gippel, C. J., I. C. O'Neill, and B. L. Finlayson (1992), The hydraulic basis for snag management, report, 116 pp., Cent. for Environ. Appl. Hydrol., Dep. of Civ. and Agric. Eng., Univ. of Melbourne, Melbourne, Victoria, Australia.

Gippel, C. J., B. L. Finlayson, and I. C. O'Neill (1996), Distribution and hydraulic significance of large woody debris in a lowland Australian river, *Hydrobiologia*, *318*, 179–194.

Gregory, S. V., K. L. Boyer, and A. M. Gurnell (Eds.) (2003), The ecology and management of wood in world rivers, *Am. Fish. Soc. Symp.*, *37*, 1–444.

Gurnell, A. M., H. Piegay, F. J. Swanson, and S. V. Gregory (2002), Large wood and fluvial processes, *Freshwater Biol.*, *47*, 601–619.

Higuchi, H., H. Sawada, and P. Van Langen (2005), Flow over a magnetically suspended cylinder in an axial free stream, paper 2005-1078 presented at the 43rd AIAA Aerospace Sciences Meeting, Am. Inst. of Aeronaut. and Astronaut., Reno, Nev.

Hoerner, S. F. (1965), *Fluid-Dynamic Drag*, 3rd ed., Midland Park, N. J.

Hoftyzer, M., and E. Dragomirescu (2010), Numerical investigation of flow behavior around inclined circular cylinders, paper presented at the Fifth International Symposium on Computational Wind Engineering, Chapel Hill, N. C., 23–27 Int. Assoc. for Wind Engineering, Kanagawa, Japan.

Hygelund, B., and M. Manga (2003), Field measurements of drag coefficients for model large woody debris, *Geomorphology*, *51*(1–3), 175–185.

Knight, D. W., K. W. H. Yuen, and A. A. I. Al-Hamid (1994), Boundary shear stress distributions in open channel flow, in *Mixing and Transport in the Environment*, edited by K. J. Beven, P. C. Chatwin, and J. H. Millbank, pp. 52–87, John Wiley, Chichester, U. K.

Knoblock, F. D. and T. Troller (1935), Tests on the effect of sidewind on the ground handling of airships, *Publ. 2*, 53–57, Daniel Guggenheim Airship Institute, Akron, Ohio.

Lamb, H. (1945), *Hydrodynamics*, Dover, New York.

Lester, R. E., and A. J. Boulton (2008), Rehabilitating agricultural streams in Australia with wood: A review, *Environ. Manage.*, *42*(2), 310–326.

Manga, M., and J. W. Kirchner (2000), Stress partitioning in streams by large woody debris, *Water Resour. Res.*, *36*(8), 2373–2379.

Manners, R. B., M. W. Doyle, and M. J. Small (2007), Structure and hydraulics of natural woody debris jams, *Water Resour. Res.*, *43*, W06432, doi:10.1029/2006WR004910.

Matsumoto, M., N. Shiraishi, M. Kitazawa, C. Knisely, H. Shirato, Y. Kim, and M. Tsujii (1990), Aerodynamic behavior of inclined circular cylinders-cable aerodynamics, *J. Wind Eng. Ind. Aerodyn.*, *33*(1–2), 63–72.

Merten, E., J. Finlay, L. Johnson, R. Newman, H. Stefan, and B. Vondracek (2010), Factors influencing wood mobilization in streams, *Water Resour. Res.*, *46*, W10514, doi:10.1029/2009WR008772.

Mutz, M. (2003), Hydraulic effects of wood in streams and rivers, *Am. Fish. Soc. Symp.*, *37*, 93–107.

Nagayama, S., and F. Nakamura (2010), Fish habitat rehabilitation using wood in the world, *Landscape Ecol. Eng.*, *6*(2), 289–305.

Naiman, R. J., G. Pinay, C. A. Johnston, and J. Pastor (1994), Beaver influences on the long-term biogeochemical characteristics of boreal forest drainage networks, *Ecology*, *75*(4), 905–921.

Ramamurthy, A. S., and C. P. Ng (1973), Effect of blockage on steady force coefficients, *J. Eng. Mech. Div. Am. Soc. Civ. Eng.*, *99*(EM4), 755–772.

Roni, P., K. Hanson, and T. J. Beechie (2008), Global review of the physical and biological effectiveness of stream habitat rehabilitation techniques, *N. Am. J. Fish. Manage.*, *28*, 856–890.

Sarpkaya, T., and M. Isaacson (1981), *Mechanics of Wave Forces on Offshore Structures*, Van Nostrand Reinhold New York.

Sear, D. A., C. E. Millington, D. R. Kitts, and R. Jeffries (2010), Logjam controls on channel:floodplain interactions in wooded catchments and their role in the formation of multi-channel patterns, *Geomorphology*, *116*, 305–319.

Seo, J. I., F. Nakamura, and K. W. Chun (2010), Dynamics of large wood at the watershed scale: A perspective on current research limits and future directions, *Landscape Ecol. Eng.*, *6*(2), 271–287.

Shaw, T. L. (1971), Effect of side walls on flow past bluff bodies, *J. Hydraul. Div. Am. Soc. Civ. Eng.*, *97*(HY1), 65–79.

Sheridan, J., J. C. Lin, and D. Rockwell (1997), Flow past a cylinder close to a free surface, *J. Fluid. Mech.*, *330*, 1–30.

Shields, F. D., Jr., and C. J. Gippel (1995), Prediction of effects of woody debris removal on flow resistance, *J. Hydraul. Eng.*, *121*(4), 341–354.

Shields, F. D., Jr., and A. D. Wood (2007), The use of large woody material for habitat and bank protection, in National Engineering Handbook [CD-ROM], part 654, *Stream Restoration Design, Tech. Suppl., 14J*, pp. TS14J-i–TS14J-13, Nat. Resour. Conserv. Serv., Washington, D. C.

Shields, F. D., Jr., S. S. Knight, and C. M. Cooper (2000), Cyclic perturbation of lowland river channels and ecological response, *Regul. Rivers Res. Manage.*, *16*(4), 307–325.

Shields, F. D., Jr., S. S. Knight, N. Morin, and J. C. Blank (2003), Response of fishes and aquatic habitats to sand-bed stream restoration using large woody debris, *Hydrobiologia*, *494*, 251–257.

Shields, F. D., Jr., N. Morin, and C. M. Cooper (2004), Large woody debris structures for sand bed channels, *J. Hydraul. Eng.*, *130*(3), 208–217.

Shields, F. D., Jr., S. S. Knight, and J. M. Stofleth (2006), Large wood addition for aquatic habitat rehabilitation in an incised sand-bed stream, Little Topashaw Creek, Mississippi, *River Res. Appl.*, *22*(7), 803–817.

Shields, F. D., Jr., S. S. Knight, and J. M. Stofleth (2008a), Stream bed organic carbon and biotic integrity, *Aquat. Conserv.*, *18*, 761–779.

Shields, F. D., Jr., S. R. Pezeshki, G. V. Wilson, W. Wu, and S. M. Dabney (2008b), Rehabilitation of an incised stream with plant materials: The dominance of geomorphic processes, *Ecol. Soc.*, *13*(2), Article 54.

Southerland, B. S., and F. Reckendorf (2010), Performance of engineered log jams in Washington State—Post project appraisal, paper presented at 2nd Joint Federal Interagency Conference on Sedimentation and Hydrologic Modeling, June 27–July 1, Las Vegas, Nev., in Joint Federal Interagency Conferences 2010: Book of Abstracts, 446 pp., ISBN 097790027X, Joint Fed. Interagency Conf., 2010, Conference on Sedimentation and Hydrologic Modeling, June 27–July 1, Las Vegas, Nev., Government Printing Office, Washington, D. C.

Spanhoff, B., and E. I. Meyer (2004), Breakdown rates of wood in streams, *J. North Am. Benthol. Soc.*, *23*(2), 189–197.

Stofleth, J., F. D. Shields Jr., and G. A. Fox (2008), Hyporheic and total hydraulic retention in small sand-bed streams, *Hydrol. Processes*, *22*, 1885–1894, doi:10.1002/hyp. 6773.

Tanaka, N., H. Takenaka, J. Yzgisawa, and T. Morinaga (2011), Estimation of drag coefficient of a real tree considering the vertical stand structure of trunk, branches and leaves, *Int. J. River Basin Manage.*, *9*(3–4), 221–230.

Temple, D. M. (1999), Flow resistance of grass-lined channel banks, *Appl. Eng. Agric.*, *15*(2), 129–133.

Thevenet, A., A. Citterio, and H. Piegay (1998), A new methodology for the assessment of large woody debris accumulations on highly modified rivers, *Regul. Rivers Res. Manage.*, *14*(6), 467–483.

Thompson, D. M. (1995), The effects of large organic debris on sediment processes and stream morphology in Vermont, *Geomorphology*, *11*, 235–244.

Triska, F. J. (1984), Role of wood debris in modifying channel geomorphology and riparian areas of a large lowland river under pristine conditions: A historical case study, *Verh. Int. Ver. Limnol.*, *22*(3), 1876–1892.

Wallerstein, N. P. (2003), Dynamic model for constriction scour caused by large woody debris, *Earth Surf. Processes Landforms*, *28*, 49–68.

Wallerstein, N. P., C. R. Thorne, and M. W. Doyle (1997), Spatial distribution and impact of large woody debris in northern Mississippi, in *Proceedings of the Conference on Management of Landscapes Disturbed by Channel Incision*, edited by S. S. Y. Wang, E. J. Langendoen, and F. D. Shields Jr., pp. 145–150, University of Mississippi, University, Miss.

Wallerstein, N. P., C. V. Alonso, S. J. Bennett, and C. R. Thorne (2001), Distorted Froude-scaled flume analysis of large woody debris, *Earth Surf. Processes Landforms*, *26*, 1265–1283.

Wallerstein, N. P., C. V. Alonso, S. J. Bennett, and C. R. Thorne (2002), Surface wave forces acting on submerged logs, *J. Hydraul. Eng.*, *128*(3), 349–353.

Ward, R. A., G. O. Brown, P. R. Weckler, D. M. Temple, F. D. Shields Jr., and C. V. Alonso (2007), Design of large wood structures in sand bed streams, paper 072241 presented at the 2007 Annual Meeting, Am. Soc. of Agric. and Biol. Eng., St. Joseph, Mich.

Webb, A. A., and W. D. Erskine (2005), Natural variability in the distribution, loading and induced scour of large wood in sand-bed forest streams, *River Res. Appl.*, *21*, 169–185.

Wilcox, A. C., J. M. Nelson, and E. E. Wohl (2006), Flow resistance dynamics in step-pool channels: 2. Partitioning between grain, spill, and woody debris resistance, *Water Resour. Res.*, *42*, W05419, doi:10.1029/2005WR004278.

Wohl, E., D. A. Cenderelli, K. A. Dwire, S. E. Ryan-Burkett, M. K. Young, and K. D. Fausch (2010), Large in-stream wood studies: A call for common metrics, *Earth Surf. Processes Landforms*, *35*, 618–625.

C. V. Alonso and F. D. Shields Jr., National Sedimentation Laboratory, ARS, USDA, PO Box 1157, 598 McElroy Dr., Oxford, MS 38655, USA. (doug.shields@ars.usda.gov)